Int J Adv Manuf Technol (2017) 89:2119–2128
DOI 10.1007/s00170-016-9218-8

ORIGINAL ARTICLE

Numerical analysis and experimental validation on multi-stage warm forging process of deep groove ball bearing—a modified punch geometry with microstructure and defect analysis

Chih-Chun Hsu[1] · **Jie-Hong Huang**[1] · **Wen-Chieh Chen**[2] · **Yiin-Kuen Fuh**[1]

Received: 26 April 2016 / Accepted: 25 July 2016 / Published online: 8 August 2016

Abstract In this study, a multi-stage warm forging process for making bearing rings is numerically and experimentally investigated. The aim of the study is to determine the crucial station of the finishing forging process such that the tool wear is prolonged and tool fracture should be minimized. In addition, in order to ensure the appropriateness of the suggested modification, a 3-dimensional finite element simulation on each sequence is performed and carefully compared with experimental investigations. Numerical simulation results indicate that the redesigned upper punch geometry, radius (R2) of the finishing forging process, demonstrate drastically different deformation rates (the effective strain/effective stress distribution) and material flow patterns, as compared with chamfer (C2) counterpart. Accuracy of the numerical models has been verified by comparing with experimental measurements. In addition, the numerically and experimentally validated process includes the detailed tooling design and dimension variation, which are of great importance in maintaining the overall structural integrity of the forging die/punch and thus, the stability of the whole process. Concerning on the waste ratio comparison, the method-used steel rods are as raw materials, and the IR/OR ring form is given by hot/warm forging and sequential cold rolling processes, and the waste ratio decreases to ~9 %. Finally, it is shown that the multi-stage warm forging process in this study could be successfully applied to the high-quantity production (10,000 pieces/h) of the IR/OR of the deep groove ball bearing with the stability and structural integrity of the whole process.

Keywords Ball bearing · Hot/warm forging · Finite element method · Experiment · Structural integrity

✉ Yiin-Kuen Fuh
michaelfuh@gmail.com

Wen-Chieh Chen
t10842130jiehong@gmail.com

[1] Department of Mechanical Engineering, National Central University, No.300, Jhongda Rd., Jhongli City, Taoyuan County 32001, Taiwan, Republic of China

[2] Tung Pei Industrial Co., Ltd., Taoyuan County 32001, Taiwan, Republic of China

1 Introduction

Bearings are routinely utilized in the various sectors of industry, including automobile, general electrical machinery, railway, aircraft, precision machinery, domestic appliances, and others. In particular, rolling bearings are the most widely used key components [1]. In terms of anatomically illustrated sense, rolling bearings are primarily composed of inner and outer rings, a set of rolling elements, securely guided in a cage and protected (sometimes hermetically) by polymeric or metallic shields [2].

In terms of production methods for rolling bearings, seamless tubes and steel rods are mainly used as the raw materials. However, seamless tubes are a huge negative factor economically, while the turning operations of the steel rod will inevitably result in the waste ratio decreases down to 9 %. The most economical way to manufacture the key components is via the metal forming process (warm forging and cold rolling processes), and the material yield can be as high as 91~93.5 %. Furthermore, forging process is also comparatively advantageous in the aspects of productivity and material grain flow of the workpiece. In addition, complex shapes can be consistently forged, at relatively fast lead time and low production cost [3–6]. Therefore, precision hot/warm forging and cold rolling processes play an important role in the bearing production [7]. Regarding product accuracy, a mass producible forged part with complicated dimensions can be mass produced and additional machining is typically

needed to satisfy the close tolerance of products [8–10]. In particular, warm/hot forging processes are favorable in the reduced forging load and diminished processing time [11, 12].

Several recent applications of precision forging were previously reported in the literature such as the outer ring of CV (constant velocity) joints with structurally forged six inner ball grooves [13]. Multi-stage warm forging and the multi-stage cold forging were successfully implemented [14]. Another example of cold forged parts is the sleeve cam of automobile start motor [15]. In order to forge big and complicated shape components with excellent mechanical attribute, isothermal forming was widely applied in aerospace industry [16]. On the various materials used in the industry, magnesium alloy AZ31B forging process of spur bevel gear was successfully carried out. [17].

Numerical simulations using a commercial software is capable of accurately predicting stress, temperature distributions, and forces during the metal forming process [18]. For example, the process design and the tool design were also carried out by a 3-dimensional finite element simulation and the key is to ensure the appropriateness of the deformation behavior [19]. Furthermore, different types of forging defect and modeling of micro-extrusion can also be performed on a commercially available software [20]. Concerning forging process for the ball bearing, however, there are very few literatures exist. One of the few literatures can be directly related to the forging process of deep groove ball bearing which investigated the various preform geometry on the final filling via the two-dimensional finite element method [21]. However, the scenarios routinely encountered in actual forging process such as geometry of punch design and related forging defects as well as flowlines still remained as a tedious experience-accumulated learning process.

In this paper, the precision forging process using SUJ2 steel billet material of the biggest bearing company in Taiwan with production capacity of 10,000 ring sets/h is analyzed. The focus will be the numerically and experimentally validated detailed tooling design and dimension variation, particularly for structural integrity of the forging die/punch. In addition, the originality of this work is primarily focused on the comparison between punch geometry of cambered and radius designs (C2 vs. R2), as validated numerically and experimentally. Furthermore, an analysis of the main types of damage on worn dies and failed parts were also identified. Design modifications and experimental validation are performed to increase in-service tooling life (primarily punch) and compared favorably with previous literatures [10, 22].

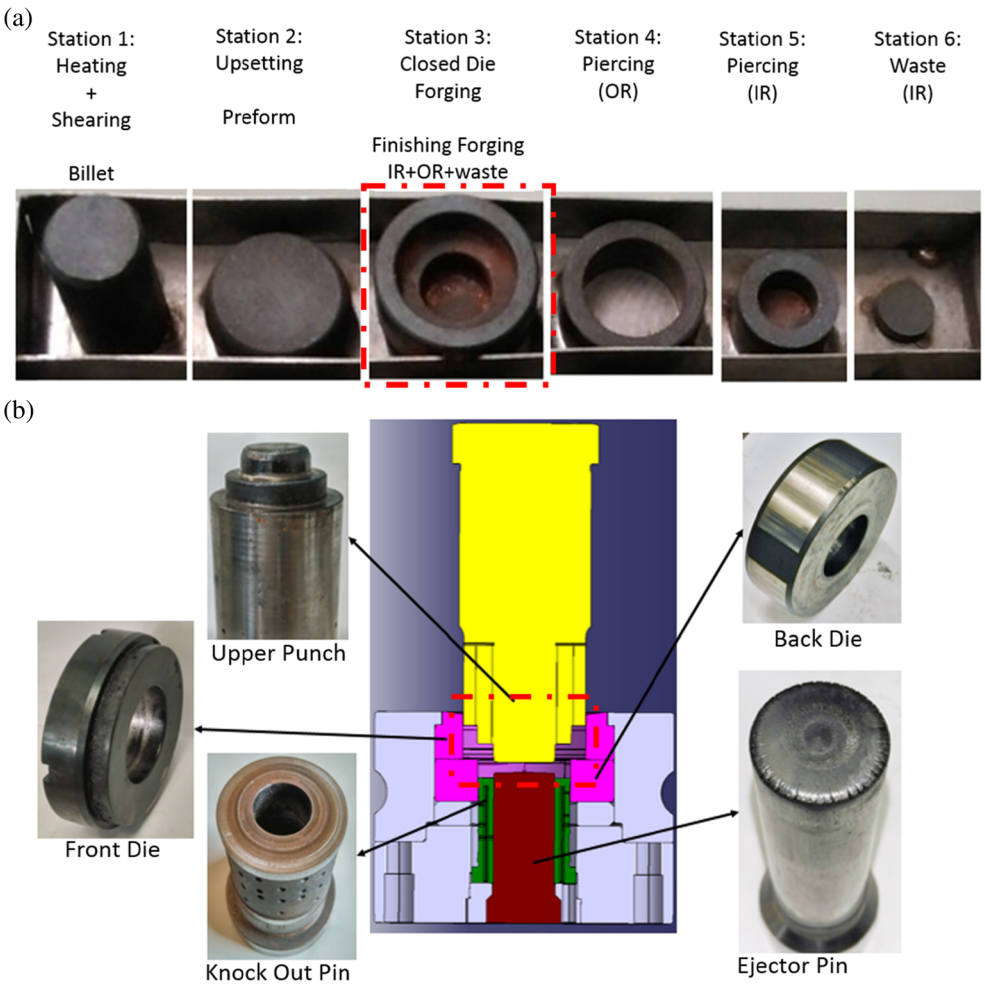

Fig. 1 Production stages of finishing forging and tooling details of finish forging stage in warm forging process. **a** The actual photos of multi-stage warm forging and **b** tooling details of finish forging stage

2 Manufacturing process for finishing forging

2.1 Traditional multi-stage warm forging

The deep groove ball bearing functions as torque transmitting device between an automotive engine and the driven wheel. The schematic of deep groove ball bearing is composed of several structural parts, such as the outer ring (OR), inner ring (IR), the rubber seal, ball, and the ball cage. In particular, the interface characteristics and surface integrity between the ball bearing/groove is of great importance to ensure the proper torque carrying capability. The multi-stage warm forging process is widely used to produce the OR and IR mainly due to the advantage of the fast cycle time and durable tooling operations. This translates into the difference in the design of finishing forging, i.e., one with ladder shape configuration as compared with pancake one before finishing forging, piercing, and separation of IR/OR parts. Concerning on the waste ratio comparison, the typical method-used steel rods are as raw material, and the IR/OR ring form is given by hot/warm forging and cold rolling processes, and the waste ratio decreases down to 9 %.

2.2 Multi-stage warm forging

In the multi-stage warm forging, the billet material is the starting workpiece and sequentially forged with the compressive deformation by the press operation. Figure 1a displayed the bearing production of all manufacturing steps, includes sheared billet, one preforming stage by upsetting operation, one fully closed die forging step at the finishing forging operation, and followed by two sequential piercing steps to remove and separate OR, IR, and waste. In the process of billet to upsetting stage, the forging temperature is set up to 1150 °C, which translates to upsetting ratio $\epsilon\epsilon_p$ = 0.53 and degree of upsetting φ_p = 0.75 (theoretically calculated as upsetting ratio $\varepsilon_p = \frac{h_0 - h_1}{h_0}$ and degree of upsetting $\varphi_p = \ln\frac{h_1}{h_0}$ can be expressed as h_0 which is the length before upset forging, h_1 in the length after upset). In particular, due to the combined effect of intense flooding of lubricating fluid and enhanced convective/conductive heat transfer between the tooling, the finishing forging process after the first stage upset forging will be significantly reduced to the warm forming range of ~950 °C, which is a critical step such that oxide scale will be minimized while the tool wear will be enhanced. Both aspects will be investigated in detail in later sections.

Table 1 Chemical Composition (wt%)

C	Mn	Si	Cr	S	P
0.95~1.10	Less than 0.5	0.15~0.35	1.3~1.6	Less than 0.025	Less than 0.025

The detailed tooling of finishing forging in bearing was presented in Fig.1b for the multi-stage warm forging process. The tooling construction is composed of the upper punch, front die, back die, ejector pin, and knock out pin. The warm forging tooling materials require the heat-resistant capability such as tooling steels of SKD61, SKH9 and SKH51/55/57. In particular, the upper punch experiences the highest forging load and temperature; therefore, the tooling wear is a significant function of

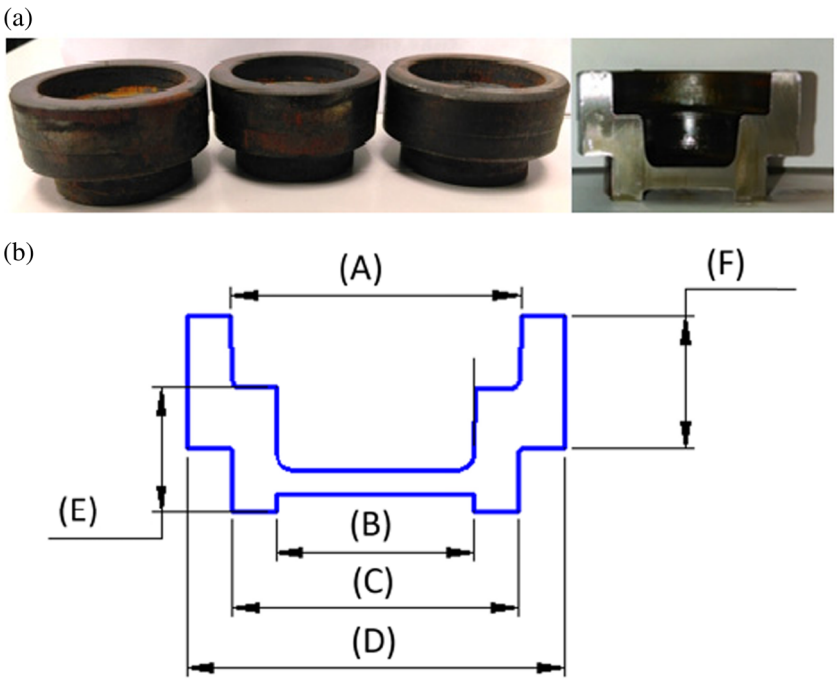

Fig. 2 **a** Optical photos of forged finishing forgings by multi-stage warm forging process (*left*) and cross-sectional view (*right*). **b** Forged detail dimensions for finishing forging. Units: mm

cooling water by water hole. Similarly, the ejector pin also shows thermal fatigue crack on the circumferential radius (initial designed as a sharp angle ~0 degree and incrementally worn out to radius ~3 mm before the replacement, after 10,000 operations) due to continuous forging operations. Ten thousand tooling life for the finishing forging is considered to be superior to the counterpart, and the main reason is attributed to the novel setup of knock out pin. Knock out pin was purposely designed to reduce the forging temperature by implementing numerous circumferential cooling passages with total numbers of 54 holes with the diameter of 2 mm.

3 Ball bearing forging process: mechanical properties and finite element model

3.1 Mechanical properties

Optical photos of forged finishing forgings by multi-stage warm forging process (left) and cross-sectional view (right), as shown in Fig. 2a. In the traditional multi-stage warm forging process for obtaining the outer ring (OR) and inner ring (IR) of the deep groove ball bearing, commonly, the forging sequence consists of six operations, which includes cutting, upsetting, closed die forging, piercing (OR and IR, separately and respectively), and disposal of waste. The heating of billets requires an operation temperature of about 1150 °C initially, cutting to the specified dimension and moved to the upsetting operation through the transfer mechanism, and the finishing forging temperature was measured of about 950 °C. Piercing and separation of IR/OR were also executed on the same equipment. All the cutting and forging processes were performed on the commercially available hot former equipment (Sakamura BP-350, composed mainly of four-die stations). The crucial specification and the layout for the finishing forging are shown in Fig. 2b. It is showing that the most critical dimensions of finishing forging, presumably contain the IR diameter (B, C)/height (E) (24.3~35.1/15.4~20.2 mm) and OR diameter (A, D)/height (F) (35.6~46.5/16.2–20.5 mm). In this design, the waste has only required a minimum size (<9 % of initial billet in weight). Comparative investigations on the finishing forging configurations were systematically performed, and the optimally available and applicable multi-stage warm process was suggested in this study.

The physical properties of SUJ2 steel are listed in the following Table 1.

The present billet material used in this study was bearing steel SUJ2, which is routinely applied to motors, ceiling fans, and application of roller bearing in a locomotive. The chemical composition in percentage by mass of SUJ2 steel material contains the following alloy elements: 0.95 to 1.10 % of carbon; 0.5 % or less of manganese; 0.15 to 0.35 % of silicon; 1.3 to 1.6 % of chromium; 0.025 % or less of sulfur, and less than 0.025 % of phosphorus, as summarized in Table 1.

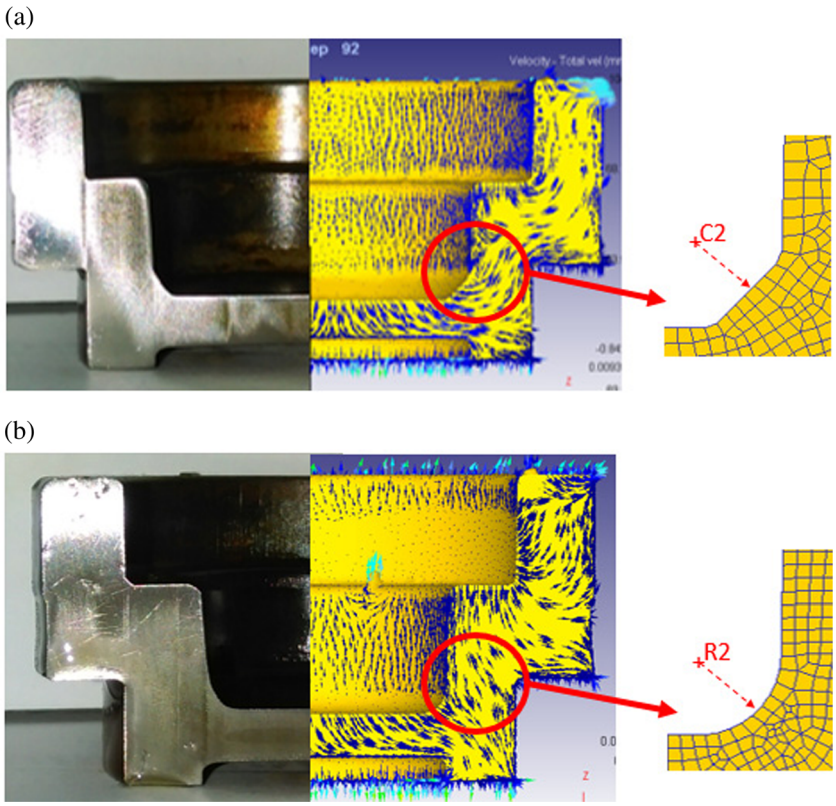

Fig. 3 Schematic view of forming and simulated models for **a** chamfer design and **b** radius design

3.2 Finite element model

In order to numerically simulate the process feasibility to concurrently obtain the OR and IR of the deep groove ball bearing under the multi-stage warm forging condition, the crucial stage of "optimal" configurations of finishing forging design was proposed and analyzed. The validity of the plastic deformation at an elevated temperature of this suggested process was numerically evaluated using the commercial finite element software, DEFORM 2D/3D simulation. The platform was an ASUS X550V workstation running the Windows 8 Ultimate x64 system. In addition, experimental investigations were also carried out for each operation and compared with the simulated results to further ensure the applicability and feasibility of the proposed design.

Figure 3 shows the schematic view of forming and simulated model for configurations of (1) chamfer (C2) and (2) radius (R2). The multi-stage warm forging process can be divided into the following steps. Initially, the punch locates at its upper limit position and the workpiece is placed on the top of the die. Secondly, the punch is pushed downward to plastically deform the workpiece. The experimental and simulated results were presented in juxtaposition. The simulated material flow can be indicated by the velocity arrow and for the configuration of (1) chamfer (C2) and (2) radius (R2) which show drastically different material flow. In particular for the case of chamfer (C2), the colliding flow was predicted and the thermal lapping was formed. The experimental validation of this defect will be presented in Fig. 7d. On the other hand, radius (R2) will improve the material flow and the defect can be minimized.

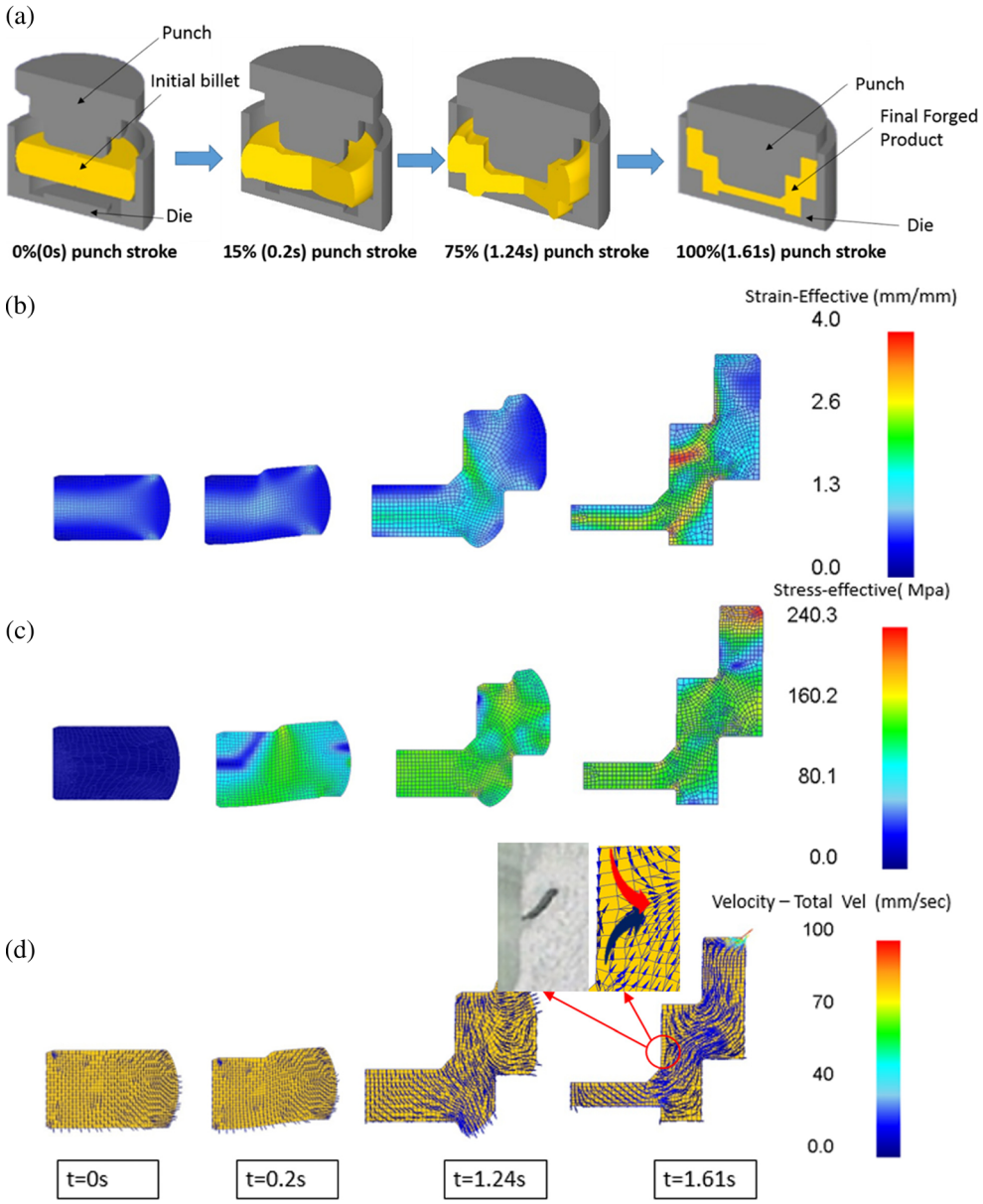

Fig. 4 Punch design of chamfer 2 (*C2*). The various simulated forging results. **a** Warm forging procedure for finish forging, **b** the effective strain distribution of forging process, **c** the effective stress distribution of forging process, and **d** the materials flow distribution of valve forging process. *Red* and *blue arrows* in the inset indicate the downward and upward material flows, respectively. The strong colliding flows as simulated and consistent with the experimental folding defect

4 Finite element simulations of finishing forging

4.1 Effect of punch design on corner chamfer 2 (C2)/radius 2 (R2)

In terms of finish forging simulation, the deformation characteristics of stress/strain at previous deformation operation are sequentially transferred to the finishing forging stage without any heat treatment. The whole finish forging simulation cycle and relevant deformation status at three punch strokes are presented in Fig. 4a. The starting billet is initially heated up to ~1150 °C; the finishing forging dimensions have to be carefully calculated by considering the coefficient of thermal expansions and associated volumetric change of the billet. At 0 % punch stroke, the upper punch moves downward in direct contact with initial billet. At 75 % punch stroke, the deformed billet is completely bounded with the inner diameter of the front/back dies and corner filling will be essential at this stage. As shown in Fig. 4a at 100 % punch stroke, final forged product is compressed up to the specified final height as determined via the incompressibility condition (volume constancy). In particular, the corner radius of upper outside diameter (OD) is fully deformed to the desired radius of 1.5 mm or less. Whereas the other corner radius such as lower inside diameter (ID)/OD is completely filled to almost sharp radius (<1 mm) due to the special tooling design (splitting of dies to prevent stress concentration).

Figure 4b, c shows the effective strain/effective stress distribution of the finishing forging process for the case of C2 punch design. At the early forging stage, the deformation mainly occurs at the contact area of the top and bottom dies. As the upper punch progressively moves downward, the maximum deformation strain occurs at the inner contact surfaces of the forging. When deformation process is completed, the effective strain of the finishing forging can reach above 1.95 over almost 60 % coverage, whereas the maximum strain reaches approximately 4, as indicated Fig. 7b. The region of maximum effective strain can be observed at the inner wall of the IR section, indicating the highest deformation. Conversely, the effective stress of the finishing forging can simulate to reach above 120 Mpa, whereas the maximum strain reaches approximately 240 Mpa.

Figure 4d shows the material flow distribution of the forging process for the design of C2. In the early stages of forging process, the material flow starts from primarily the axial metal resistance and progressively transforming into radial flow pattern, minimizing the flow resistance. Subsequently, as the height of the billet decreases, diameter and surface area of

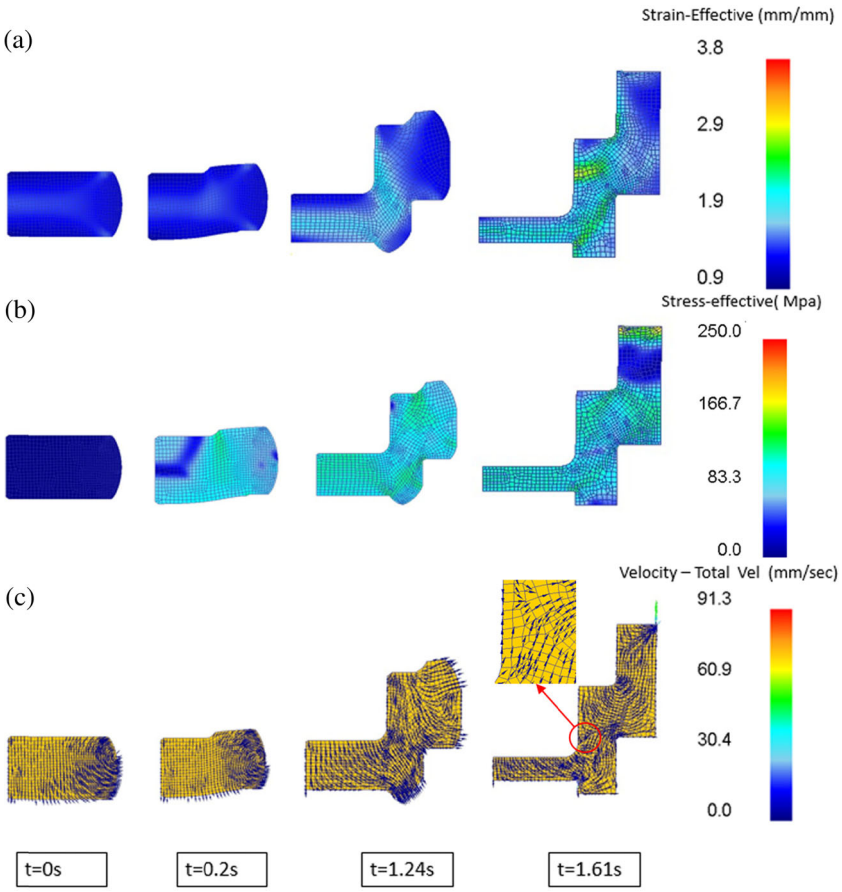

Fig. 5 Punch design of radius 2 (*R2*). The various simulated forging results. **a** The effective strain distribution of forging process, **b** the effective stress distribution of forging process, and **c** the material flow distribution of valve forging process. The colliding material is highly alleviated

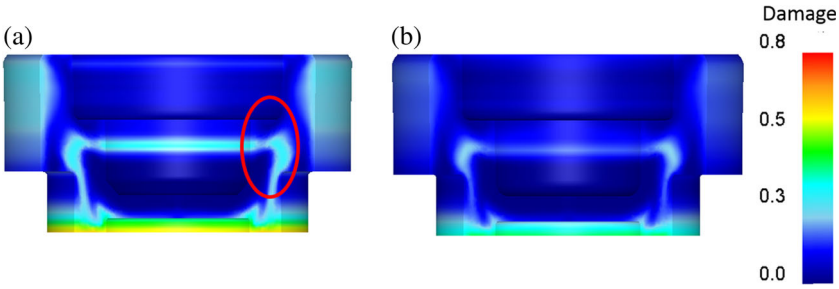

Fig. 6 Distribution of damage on finishing forging. **a** Chamfer 2 of finishing forging and b radius 2 of finishing forging

the forging expand rapidly to completely fill the die cavity, as resulted in the higher die resistance. It was shown that the colliding flow was numerically predicted as indicated at the inset, and thermal lapping will be formed. The actual forging experiment also confirmed the defect, as shown in zoom-up inset.

Similarly, the various forging stages of punch design of radius 2 (R2) are also simulated and the evolution of effective strain/stress is shown in Fig. 5a, b. Again, four sequential stages were simulated and corresponded in the loaded to the case of C2 design. At the final stage ($t = 1.61$ s), when forging is completed, the effective strain of the finishing forging is comparable to C2 design, whereas the maximum strain reaches approximately 3.8. Similar case can be found on the effected stress distribution. The most remarkable difference between chamfer (C2) and radius (R2) lies on the material flow pattern. Figure 5c shows the materials flow distribution of the forging process about R2. In contrary to chamfer (C2) design, the radius (R2) design shows a much smooth flow pattern with significantly less colliding flow, as indicated in the velocity arrow. Thus, the improved material flow of R2 design can minimize the defect such as thermal lapping.

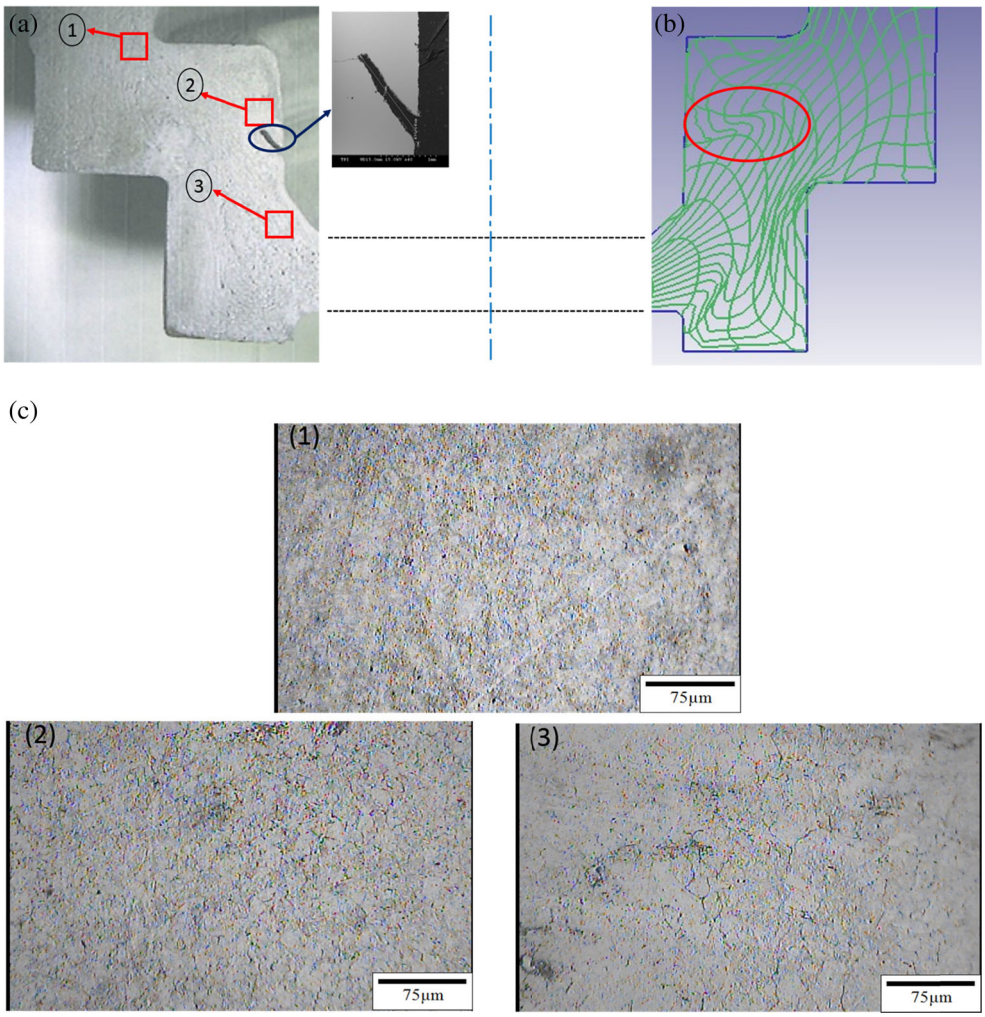

Fig. 7 Experimental and simulated results for chamfer 2 (*C2*) finishing forging. **a** The experimental results, and the *blue circle* is the sem image of the crack of the finishing forging; **b** the FEM results of metal flow lines. The *center line* is indicated in the figure. **c** The selected region of the grain size distribution after forging, point 1 (the average grain size of 7.35 μm), point 2 (the average grain size of 5.30 μm), and point 3 (the average grain size of 7.22 μm)

Furthermore, the absolute critical damage is analyzed for the geometry of finishing forging of C2/R2 design, respectively. Figure 6a, b shows the distribution of damage on finishing forging of C2/R2 design of finishing forging. It is clearly simulated that C2 design in the inner ring beared higher damage concentration than the R2 design, as indicated by the red ellipse. Incidentally, the region of maximum damage coincides with the effective strain at the inner wall of the IR section, which is in agreement with the highest deformation and experimentally observed forging defect.

4.2 Results and discussion of forging results

The flow line pattern of finishing forging is further analyzed by wire electrical discharge machining (EDM) cutting along the center axis. Microstructure observation is performed by etching 0.7 % picric acid with 99.3 % alcohol solution.

Etching time was conducted at room temperature (25 °C) for 15–20 s and rinsed with water and drying step. Figure 7 shows the experimental and simulated results for chamfer 2 (C2) finishing forging.

The flow line graph of the cross section in Fig. 7a demonstrates that the inner ring has a severe crack oriented at 45° with the inner wall, which is unacceptable and needs to be modified, and the blue circle is the sem image of the crack of the finishing forging. A scanning electron microscope (SEM) electron image of finishing forging is investigated from the region of lapping defect, and a long slender crack can be clearly observed on the SEM image as demonstrated. The working distance of 20 mm was chosen for reasonable irradiation of the detector by the secondary electrons. The specimen defect of finishing forging was observed, and the width of edge crack was measured about 490 μm and the length of crack ~1.76 mm. The frequency of this defect is about 33 % for the C2 design, and the possible reason is primarily attributed to poor material flow and resulted in excessive effective stress/strain. Therefore, the design of radius 2 (R2) is attempted to smooth out the material flow pattern and minimize the lapping defect. On the other hand, as indicated in Fig. 7b, the distorted flow lines can be identified on the inset. Figure 7c shows the metallographic microstructure for the cross section of the chamfer 2 (C2) finishing forging with

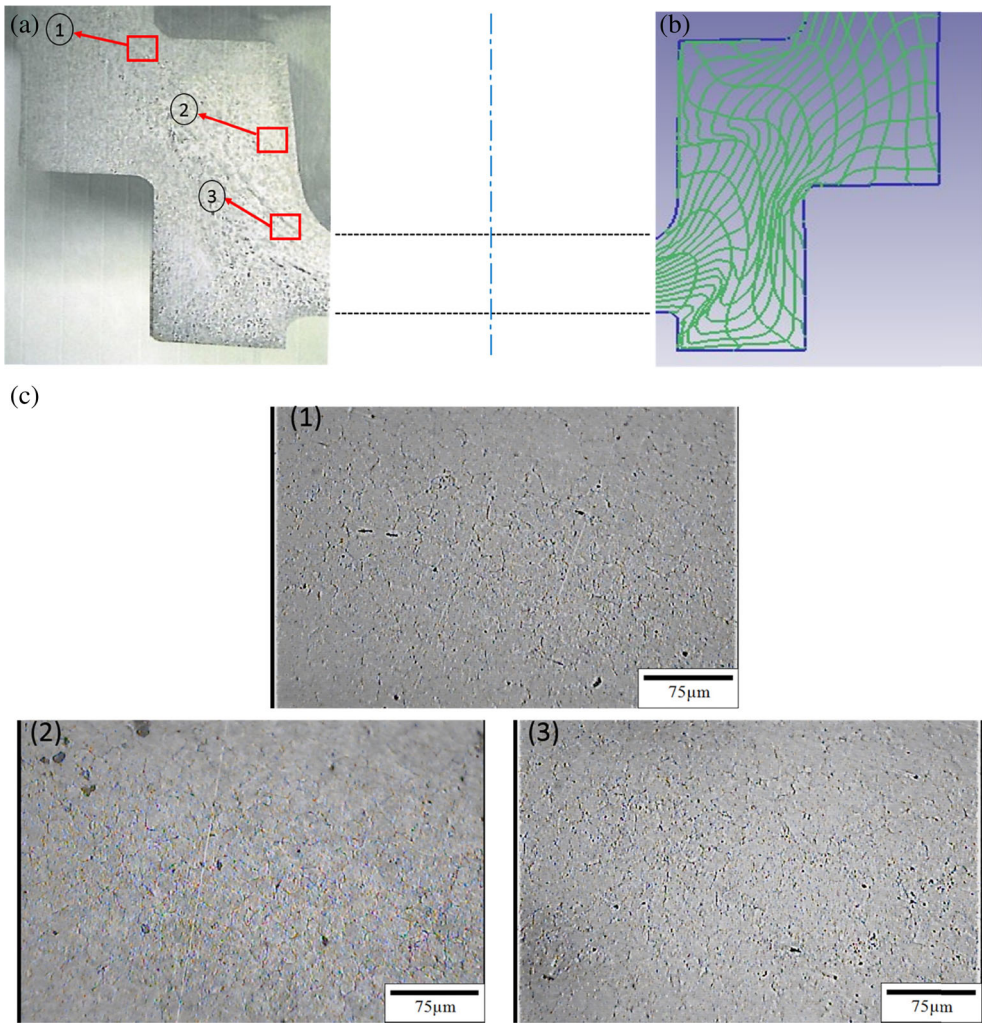

Fig. 8 Experimental and simulated results for radius 2 (*R2*) finishing forging. **a** The experimental results, **b** the FEM results of metal flow line, and **c** metallographic microstructure of the specimen after forging. Point 1 (the average grain size of 7.50 μm), point 2 (the average grain size of 5.93 μm), and point 3 (the average grain size of 7.65 μm)

grain size distribution after forging, point 1 (the average grain size ~7.35 μm), point 2 (the average grain size ~5.30 μm), and point 3 (the average grain size ~7.22 μm). This result illustrates that the grain size varies modestly from 5.30 to 7.35 μm, mainly due to the effective strain experienced during the forming process.

In comparison, Fig. 8a, b shows the comparison for the design of radius 2 (R2) finishing forging. The graph demonstrates that the flow line of the finishing forging is improved significantly and no defect occurred. The simulated flow line is comparatively undistorted and uniform, as compared to the counterpart of C2 design.

Figure 8c also shows the metallographic microstructure of the specimen after forging, point 1 (the average grain size of 7.50 μm), point 2 (the average grain size of 5.93 μm), and point 3 (the average grain size of 7.65 μm). Basically, the grain size distribution is rather similar for both designs of C2/R2, indicating the negligently small impact for radius/chamfer design. However, the flow line of R2 design is ameliorated by maintaining uninterrupted material flow at the critical region, which guarantees defect-free product with continuous grain flow and higher mechanical properties of this forging. Similarly, three points were selected/ to observe the microstructure, with particular focus on the evolution of grain size (Fig. 8c). In general, the average grain size of R2 is more uniform than the C2 counterpart, mainly attributed to the continuously maintained flow line.

5 Conclusion

In this study, the multi-stage warm forging process for obtaining the finishing forging of the IR/OR deep groove ball bearing was analyzed, numerically and experimentally. The numerical verifications is performed by using finite element program, DEFORM 3D™. A series of experimental investigations were also successfully performed, primarily the critical region of interest on the punch at the finishing forging stage. In summary, the following results can be concluded:

(1) The bearing of the finishing forging process was simulated based on the rigid plastic finite element of bearing material SUJ2. In the process of billet to upsetting, the forging temperature is initially set up to 1150 °C, which translates to upsetting ratio $\epsilon_p = 0.53$ and degree of upsetting $\varphi_p = 0.75$. In particular, the temperature of finishing forging process after the first stage upset forging will be significantly reduced to the warm forming range of ~950 °C, which is a critical step such that oxide scale will be minimized while the tool wear will be aggravated.

(2) For the designs of chamfer (C2) and radius (R2) of the finishing forging punch, the effective strain/effective stress distribution demonstrates drastically different deformation rate and material flow pattern. The R2 design shows a significantly smooth flow pattern with relatively less colliding flow, as indicated in the velocity arrow than the C2 counterpart. Thus, the improved material flow of R2 design can minimize the defect such as thermal lapping.

(3) The experimentally obtained average grain size of R2 design is comparatively uniform than the C2 counterpart, i.e., C2: 5.30~7.35 μm and R2: 5.93~7.65 μm. In general, the average grain size of R2 is more uniform than the C2 counterpart, mainly attributed to the continuously maintained flow line. However, the grain size distribution is rather similar such that the negligently small effect for radius/chamfer design can be concluded. However, the flow line of R2 design is ameliorated by maintaining uninterrupted material flow at the critical region.

(4) In terms of the material yield for the analyzed IR/OR forging parts, the multi-stage warm forging process could significantly reduce the material waste ~9 % of the initial weight. The saving is significant since the precision forging process using SUJ2 steel billet material belongs to the biggest bearing company in Taiwan with a production capacity of 10,000 ring sets/h. The numerically and experimentally validated process includes the detailed tooling design, and dimension variation is of great importance in maintaining the overall structural integrity of the forging die/punch and thus, the stability of the whole process.

Acknowledgments This work was supported by the Tung Pei Industrial Co., Ltd. through the grant number 10313124. And, the last author would like to acknowledge the financial support of TPI, Taoyuan, Taiwan. In addition, the generous gift of scholarship and internship was highly appreciated through this industry-university cooperation.

References

1. Chao W, Ton B, Edin O, Viktor R, Bert G (2014) Influence of feed rate on damage development in hot ring rolling. Procedia Eng 81: 292–297
2. Ke Y, Ning W, Qiang Z, Yongsheng Z, Jinhua Z, Qingbo N (2015) Theoretical and experimental investigation on the thermal characteristics of double-row tapered roller bearings of high speed locomotive. Int. J. Heat Mass Transf 84:1119–1130
3. Prasad Y, Rao KP (2011) Materials modeling and finite element simulation of isothermal forging of electrolytic copper. Mater Des 32:1851–1858
4. Kim EZ, Oh SI, Lee YS, Na KH (2008) Backward can extrusion of ultra-fine-grained bulk Al–Mg alloy fabricated by cryomilling and hydrostatic extrusion. Backward can extrusion of ultra-fine-grained bulk Al–Mg alloy fabricated by cryomilling and hydrostatic extrusion J Mater Process Technol 201:163–167
5. Kamouneh A, Jun N, Stephenson D, Vriesen R, DeGrace G (2007) Diagnosis of involutometric issues in flat rolling of external helical

gears through the use of finite-element models. Int J of Mach Tools and Manuf 47:1257–1262
6. Kroiß T, Engel U, Merklein M (2013) Comprehensive approach for process modeling and optimization in cold forging considering interactions between process, tool and press. J Mater Process Technol 213: 1118–1127
7. Yuan L, Zhao Z, Shi W, Xu F, Shan D (2015) Isothermal forming of the large-size AZ80A magnesium alloy forging with high mechanical properties. Int J Adv Des Manuf Technol 78:2039–2047
8. Faraji G, Jafarzadeh H, Jeong HJ, Mashhadi MM, Kim HS (2012) Umerical and experimental investigation of the deformation behavior during the accumulative back extrusion of an AZ91 magnesium alloy. Mater Des 35:251–258
9. Ku TW, Kang BS (2014) Tool design for inner race cold forging with skew-type cross ball grooves. J Mater Process Technol 214: 1482–1502
10. Lee MC, Chung SH, Jang SM, Joun MS (2009) Three-dimensional simulation of forging using tetrahedral and hexahedral elements. Fin Ele Anal Des 45:745–754
11. Xinbo L, Hongsheng X, Zhiliang Z (2003) Flow stress of carbon steel 08F in temperature range of warm-forging. J Mater Process Technol 139:543–546
12. Ou H, Lan J, Armstrong CG, Price MA (2004) An FE simulation and optimization approach for the forging of aeroengine components. J Mater Process Technol 151:208–216
13. Wan KT, Ho KL, Soo KB (2013) Multi-stage cold forging and experimental investigation for the outer race of constant velocity joints. Mater Des 49:368–385
14. Ku TW, Kim LH, Kang BS (2014) Process simplification of multi-stage forging for the outer race of a CV joint. Mater Manuf Process 29:85–92
15. Kang GJ, Kim J, Kang BS (2008) Numerical and experimental evaluation for elastic deformation of a cold forging tool and workpiece for a sleeve cam of an automobile start motor. Mech Eng 222: 217–224
16. Puertas I, Pérez C, Salcedo D, León J, Fuertes JP, Luri(2013) Design and mechanical property analysis of AA1050 turbine blades manufactured by equal channel angular extrusion and isothermal forging. Mater Des 52:885–784
17. Juan L, Zhenshan C (2009) Hot forging process design and parameters determination of magnesium alloy AZ31B spur bevel gear. J Mater Process Technol 209:5871–5880
18. Hongchao J, Jinping L, Baoyu W, Zhengrong Z, Tao Z, Zhenghuan H (2015) Numerical analysis and experiment on cross wedge rolling and forging for engine valves. J Mater Process Technol 221:223–242
19. Duarte M, Martins H (2004) Inner joint forming and pullout simulation using finite element analysis. SAE Tech Paper 01:3422
20. Chan WL, Fu MW, Lu J (2011) Experimental and simulation study of deformation behavior in micro-compound extrusion process. Mater Des 32:525–534
21. Murat A, Tekkaya A, Özhan F (2005) Comparison of various preforms for hot forging of bearing rings, journal of materials processing technology. J Mater Process Tech 169:72–82
22. Lavtar L, Muhič T, Kugler G, Terčelj M (2011) Analysis of the main types of damage on a pair of industrial dies for hot forging car steering mechanisms. Eng Failure Anal 18:1143–1152